

# Globular clusters in the inner Galaxy classified from dynamical orbital criteria

Angeles Pérez-Villegas,<sup>1</sup>[★](#) Beatriz Barbuy,<sup>1</sup> Leandro Kerber,<sup>2</sup> Sergio Ortolani<sup>3</sup>  
Stefano O. Souza<sup>1</sup> and Eduardo Bica,<sup>4</sup>

<sup>1</sup>Universidade de São Paulo, IAG, Rua do Matão 1226, Cidade Universitária, São Paulo 05508-900, Brazil

<sup>2</sup>Universidade Estadual de Santa Cruz, Rodovia Jorge Amado km 16, Ilhéus 45662-000, Brazil

<sup>3</sup>Dipartimento di Fisica e Astronomia ‘Galileo Galilei’, Università di Padova, Vicoletto dell’Osservatorio 3, Padova, I-35122, Italy

<sup>4</sup>Universidade Federal do Rio Grande do Sul, Departamento de Astronomia, CP 15051, Porto Alegre 91501-970, Brazil

Accepted XXX. Received YYY; in original form ZZZ

## ABSTRACT

Globular clusters (GCs) are the most ancient stellar systems in the Milky Way. Therefore, they play a key role in the understanding of the early chemical and dynamical evolution of our Galaxy. Around 40% of them are placed within  $\sim 4$  kpc from the Galactic center. In that region, all Galactic components overlap, making their disentanglement a challenging task. With Gaia DR2, we have accurate absolute proper motions for the entire sample of known GCs that have been associated with the bulge/bar region. Combining them with distances, from RR Lyrae when available, as well as radial velocities from spectroscopy, we can perform an orbital analysis of the sample, employing a steady Galactic potential with a bar. We applied a clustering algorithm to the orbital parameters apogalactic distance and the maximum vertical excursion from the plane, in order to identify the clusters that have high probability to belong to the bulge/bar, thick disk, inner halo, or outer halo component. We found that  $\sim 30\%$  of the clusters classified as bulge GCs based on their location are just passing by the inner Galaxy, they appear to belong to the inner halo or thick disk component, instead. Most of GCs that are confirmed to be bulge GCs are not following the bar structure and are older than the epoch of the bar formation.

**Key words:** Galaxy: globular clusters: general – Galaxy: bulge – Galaxy: kinematics and dynamics

## 1 INTRODUCTION

The orbital evolution of globular clusters (GCs) in the Galaxy, combined with kinematics and stellar population analyses, can provide important information to decipher the history of our Galaxy. In Bica et al. (2016) 43 clusters were selected as related to the bulge component based on their location. Recently, Bica et al. (2019) compiled 200 GCs in the Galaxy, adding new entries such as the recently detected ones in the Vista Variables in the Via Lactea (Saito et al. 2012) survey by Minniti et al. (2017a,b). By including confirmed GCs plus candidates, the number rises to 294 objects, thus reducing the lack of the Galactic GCs with respect to M31 (Caldwell & Romanowsky 2016).

The stellar population components in the Galaxy have been under scrutiny in the last decades. The Galactic disk and halo are well established, and the existence of a thick

disk is increasingly more confirmed. As for the Galactic bulge configuration as an entity, it still is under definition. In early work, a sample of metal-rich GCs with a flattened distribution were identified as disk GCs by Zinn (1980, 1985). The properties of this disk system of metal-rich GCs were described by Armandroff (1989), to have a scale height between 0.8 to 1.5 kpc, a rotational velocity of  $193 \pm 29$  km s<sup>-1</sup>, and a line-of-sight velocity dispersion of  $59 \pm 14$  km s<sup>-1</sup>, concluding that these parameters are consistent with properties of thick-disk stars. Later, Frenk & White (1982), Minniti (1995), and Côté (1999) deduced that metal-rich GCs within 3 kpc from the Galactic center, should be associated to the Galactic bulge rather than to the thick disk, based on kinematics, spatial distribution and metallicity.

The Galactic bulge formation is under study in several contexts. Barbuy et al. (2018a) list the following possible scenarios: a) bulge and thick disk were formed early on simultaneously through strong gas accretion; b) hierarchical merging of subclumps; c) merging of early thick-disk sub-

\* E-mail: mperez@iag.usp.br

clumps; d) a major merger; e) secular evolution of the bar; f) dwarf galaxies accretion. There is also the hypothesis of the oldest stellar populations in the Galactic bulge to be seen as an extension of the inner halo in the innermost Galaxy.

The dynamical properties and their orbits provide further information that would help allocating the objects to a given stellar population. With the recently available Gaia Data Release 2 (DR2; [Gaia Collaboration 2018a](#)), the investigation of cluster orbits is made timely. Previously this kind of work was attempted for the bulge clusters, by [Dinescu et al. \(2003\)](#). More recently [Pérez-Villegas et al. \(2018\)](#) and [Rossi et al. \(2015b\)](#) derived proper motions and orbits for 9 inner bulge clusters.

In the present work we study a sample of bulge GCs, plus the intruders or outsiders from [Bica et al. \(2016\)](#), their Tables 1 and 2). In order to compute orbits, reliable radial velocities, proper motions, and distances are needed. Radial velocities, that can only be derived from spectroscopy, are still missing for about a dozen of these clusters, making that 78 of them can be studied. The dynamical parameters perigalactic and apogalactic distances, maximum height from the plane and eccentricity, are derived such that their appartenance to different Galaxy components are identified.

In Sect. 2 the sample and available data are described. In Sect. 3 the Galactic model potential is detailed. In Sect. 4 dynamical properties of the orbits are discussed, and in Sect. 5 the globular clusters are classified. The bulge globular clusters are further discussed in Sect. 6, and conclusions are drawn in Sect. 7.

## 2 DATA

The sample includes 40 GCs from the list of bulge globular clusters by [Bica et al. \(2016\)](#), their Table 1), for which radial velocities are available. Another 37 GCs from the outer shell and clusters somewhat farther, at distances  $3.0 < d_{\text{GC}} < 4.5$  kpc and some clusters with  $d_{\text{GC}} > 4.5$  kpc from the Galactic center ([Bica et al. 2016](#), their Table 2), and the halo GC NGC 6752 are also added, with the purpose of identifying differences in the orbital properties among clusters that belong to each Galactic component. Figure 1 shows the location in Galactic coordinates of our total sample that contains 78 clusters.

In Table 1, we list the cluster parameters employed in this study. Equatorial ( $\alpha, \delta$ ) and Galactic ( $l, b$ ) coordinates are given in Columns 2 to 5. The heliocentric distance  $d_{\odot}$ , in Column 6 is taken from Colour-Magnitude Diagrams (CMDs) and RR Lyrae star distance determination for the clusters HP 1, Terzan 10, NGC 6522, NGC 6626, NGC 6558, Djorgovski 1, Djorgovski 2, NGC 6304, NGC 6624, NGC 6637, NGC 6652, NGC 6717, NGC 6723, and NGC 6362 ([Kerber et al. 2018](#); [Barbuy et al. 2018b](#); [Kerber et al. 2019](#); [Ortolani et al. 2019a,b](#), Oliveira et al. in prep.) that we consider reliable. For the others, distances from [Harris \(1996](#), edition of 2010, hereafter H10), or [Baumgardt et al. \(2019\)](#) were adopted. Radial velocities  $V_r$ , given in Column 7, are taken from spectroscopy analyses from the literature. The absolute proper motions (PMs),  $\mu_{\alpha}^* = \mu_{\alpha} \cos \delta$ ,  $\mu_{\delta}$ , in Column 8 and 9, are the values estimated from the Gaia DR2 ([Gaia Collaboration et al. 2018b](#)) and for the clusters marked with a star we calculated the PMs following the procedure

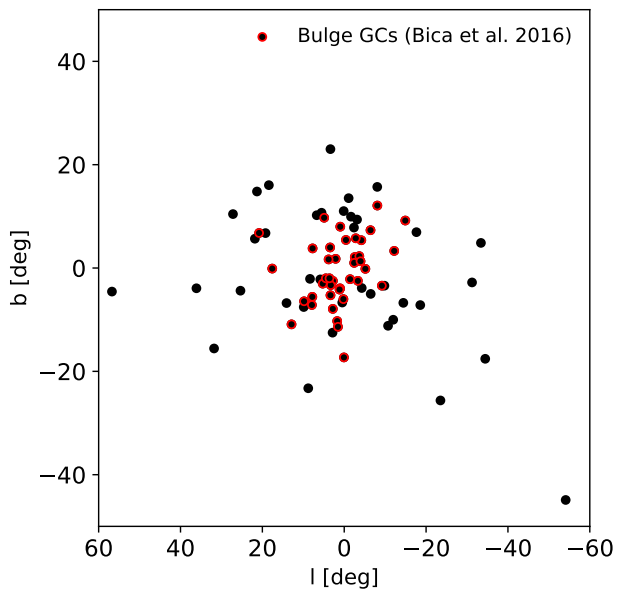


**Figure 1.** Location in Galactic coordinates of the GCs analyzed. Red open circles are the clusters classified as bulge GCs in [Bica et al. \(2016\)](#).

explained below, the uncertainties of PMs include the systematic error of  $0.035 \text{ mas yr}^{-1}$  reported by the [Gaia Collaboration et al. \(2018b\)](#). The metallicities, given in Column 10, available from high-resolution studies reported in [Bica et al. \(2016](#), their Table 3), [Barbuy et al. \(2014, 2018b\)](#) for NGC 6522 and NGC 6558, derivations from literature and isochrone fittings to Colour-Magnitude Diagrams from our group (Oliveira et al. 2019, in preparation), and for the remaining clusters the values are adopted from the website by Bruno Dias <sup>1</sup>. Column 11 gives the core radius taken from H10.

For the proper motion derivation from Gaia DR2, we selected the individual stars with the astrometric information including positions and PMs within 5 arcmin from the cluster center. We removed the stars with PM errors  $> 0.25 \text{ mas yr}^{-1}$ . Then, stars in each cluster were retrieved, within the core radius of each cluster from H10 to estimate the PMs. A selection of member stars was carried out with a combined plot of PMs in both directions, and through a Gaussian mixture model, as shown in Fig. 2, in order to get the mean PM in each direction and uncertainties. We applied this method to 32 GCs of our sample, and the PM determinations for them are inside  $1-\sigma$  compared with those estimated by [Gaia Collaboration et al. \(2018b\)](#), [Vasiliev \(2019\)](#), and [Baumgardt et al. \(2019\)](#), except for Terzan 1 and Terzan 5, that are inside  $3-\sigma$ . The PMs for the remaining clusters are taken from the new PM determination of GCs using Gaia DR2 from the references above.

<sup>1</sup> <http://www.sc.eso.org/~bdias/catalogues.html>



Palomar 11	296.31	-8.01	31.80	-15.57	$14.30 \pm 1.40^e$	$-67.64 \pm 0.76^e$	$-1.79 \pm 0.05$	$-4.94 \pm 0.05$	-0.35	1.19
Palomar 6*	265.93	-26.22	2.10	1.78	$5.80 \pm 0.58^e$	$177.00 \pm 1.00^i$	$-9.11 \pm 0.06$	$-5.27 \pm 0.06$	$-1.00^m$	0.66
Palomar 7	272.68	-7.20	21.83	5.67	$5.39 \pm 0.51^e$	$155.06 \pm 0.69^e$	$-2.47 \pm 0.05$	$-4.41 \pm 0.05$	-0.53	1.01
Palomar 8	280.37	-19.82	14.10	-6.78	$12.80 \pm 1.28^e$	$-41.14 \pm 1.81^e$	$-2.04 \pm 0.04$	$-5.64 \pm 0.04$	-0.34	0.56
Terzan 1*	263.95	-30.47	357.57	1.00	$6.70 \pm 0.67$	$63.00 \pm 0.50^i$	$-3.02 \pm 0.05$	$-4.49 \pm 0.04$	$-1.26^m$	0.04
Terzan 10	270.74	-26.06	4.49	-1.99	$10.40 \pm 1.00^a$	$208.60 \pm 3.20^e$	$-7.02 \pm 0.07$	$-2.51 \pm 0.06$	-0.97	0.90
Terzan 12	273.06	-22.74	8.36	-2.10	$3.40 \pm 0.34^e$	$94.77 \pm 0.97^e$	$-6.07 \pm 0.07$	$-2.63 \pm 0.07$	-0.47	0.83
Terzan 2*	261.89	-30.80	356.32	2.30	$7.50 \pm 0.75^d$	$144.60 \pm 0.80^d$	$-2.21 \pm 0.06$	$-6.16 \pm 0.05$	-0.42	0.03
Terzan 3*	247.17	-35.35	345.08	9.19	$8.20 \pm 0.82^d$	$-135.76 \pm 0.57^e$	$-5.61 \pm 0.04$	$-1.69 \pm 0.04$	-0.96	1.18
Terzan 4	262.66	-31.59	356.02	1.31	$6.70 \pm 0.67^e$	$-39.93 \pm 3.76^e$	$-5.60 \pm 0.07$	$-2.60 \pm 0.12$	$-1.60^m$	0.90
Terzan 5*	267.02	-24.81	3.81	1.67	$5.50 \pm 0.51^e$	$-81.40 \pm 1.36^e$	$-1.35 \pm 0.07$	$-4.44 \pm 0.06$	-0.40	0.16
Terzan 6*	267.69	-31.28	358.57	-2.16	$6.80 \pm 0.68^d$	$137.15 \pm 1.70^e$	$-5.70 \pm 0.11$	$-7.20 \pm 0.11$	-0.53	0.05
Terzan 9*	270.41	-26.84	3.61	-1.99	$7.10 \pm 0.71^d$	$71.40 \pm 0.40^i$	$-2.19 \pm 0.06$	$-7.47 \pm 0.05$	-1.08	0.03
Ton 2*	264.04	-38.55	350.80	-3.42	$6.40 \pm 0.64^e$	$-172.70 \pm 0.30^i$	$-5.92 \pm 0.05$	$-0.55 \pm 0.05$	-0.26	0.54

**References.** <sup>a</sup> Ortolani et al. (2019a); <sup>b</sup> Ortolani et al. (2019b); <sup>c</sup> Kerber et al. (2019); <sup>d</sup> Harris (1996, updated in 2010), <sup>e</sup> Baumgardt et al. (2019); <sup>f</sup> Oliveira et al. (2019, in preparation); <sup>g</sup> Kerber et al. (2018); <sup>h</sup> Barbuy et al. (2018b); <sup>i</sup> Vásquez et al. (2018); <sup>j</sup> Barbuy et al. (2016); <sup>k</sup> Dias et al. (2016); <sup>l</sup> Barbuy et al. (2014); <sup>m</sup> Bica et al. (2016, their Table 3). <sup>†</sup>Metallicities with no reference come from the website by Bruno Dias (<http://www.sc.eso.org/~bdias/catalogues.html>). <sup>‡</sup>  $R_c$  taken from H10.

Table 2: Globular Cluster distances from the literature.

Cluster	Adopted (kpc)	H10 (kpc)	Baumgardt+19 (kpc)	Valenti+07,10 (kpc)	Gaia (1/plx) (kpc)	Our Group (kpc)	Bica+06 (kpc)
BH 261	$6.50 \pm 0.65$	6.50	6.50	—	—	—	—
Djorg 1*	$9.30 \pm 0.50$	13.70	13.70	13.50	—	9.30	8.80
Djorg 2*	$8.75 \pm 0.20$	6.30	6.30	7.0	9.60	8.75	6.70
ESO452SC11*	$6.50 \pm 0.65$	8.30	6.50	—	—	—	7.8
HP 1	$6.59 \pm 0.16$	8.20	6.80	6.80	50.0	6.59	7.40
Liller 1	$8.20 \pm 0.82$	8.20	8.10	7.90	—	7.60	10.50
Lynga 7	$8.0 \pm 0.80$	8.0	8.0	—	—	—	7.2
Mercer 5	$5.50 \pm 0.55$	—	5.50	—	—	—	—
NGC 104	$4.50 \pm 0.45$	4.50	4.43	—	5.10	—	4.50
NGC 5927*	$8.16 \pm 0.27$	7.70	8.16	—	10.04	—	7.60
NGC 6139	$9.80 \pm 0.83$	10.10	9.8	—	—	—	10.1
NGC 6144	$8.90 \pm 0.89$	8.90	8.90	—	14.97	—	10.30
NGC 6171	$6.03 \pm 0.31$	6.40	6.03	—	6.76	—	6.40
NGC 6235*	$13.52 \pm 1.35$	11.50	13.52	—	16.18	—	10.00
NGC 6256*	$6.40 \pm 0.64$	10.30	6.40	9.10	—	6.4	6.60
NGC 6266	$6.41 \pm 0.12$	6.80	6.41	6.6	4.57	—	6.90
NGC 6273	$8.27 \pm 0.41$	8.80	8.27	8.20	10.82	—	8.70
NGC 6284	$15.3 \pm 1.53$	15.3	15.14	—	20.04	—	14.70
NGC 6287	$9.40 \pm 0.94$	9.40	9.40	—	9.31	—	8.50
NGC 6293	$9.23 \pm 0.70$	9.50	9.23	10.50	14.37	—	8.80
NGC 6304	$6.28 \pm 0.11$	5.9	5.77	6.0	9.29	6.19	6.10
NGC 6316*	$11.60 \pm 1.16$	10.40	11.60	11.6	15.17	—	11.00
NGC 6325	$7.80 \pm 0.78$	7.80	7.80	—	6.99	6.90	9.60
NGC 6333	$8.40 \pm 0.84$	7.90	8.40	—	10.70	—	8.20
NGC 6342	$8.43 \pm 0.84$	8.50	8.43	8.40	10.28	—	8.60
NGC 6352	$5.89 \pm 0.58$	5.60	5.89	—	6.48	—	5.70
NGC 6355	$8.70 \pm 0.87$	9.20	8.70	9.0	—	8.80	7.20
NGC 6356	$15.10 \pm 1.51$	15.10	15.10	—	12.64	15	15.20
NGC 6362	$7.69 \pm 0.13$	7.6	7.36	—	10.27	7.71	8.10
NGC 6366	$3.66 \pm 0.20$	3.5	3.66	—	4.36	—	3.60
NGC 6380*	$9.80 \pm 0.98$	10.90	9.80	9.20	9.86	9.8	10.70
NGC 6388*	$10.74 \pm 0.12$	9.90	10.74	11.9	20.74	—	11.50
NGC 6401*	$7.7 \pm 0.77$	10.6	7.7	7.7	8.65	12.0	7.70
NGC 6402	$9.31 \pm 0.44$	9.30	9.31	—	18.66	—	8.90
NGC 6440	$8.24 \pm 0.82$	8.5	8.24	8.20	10.43	8.47	8.40
NGC 6441	$11.83 \pm 0.14$	11.60	11.83	13.5	24.81	—	11.20
NGC 6453	$11.60 \pm 1.16$	11.60	11.60	10.7	23.53	8.5	11.20

NGC 6496	$11.30 \pm 1.13$	11.30	11.30	—	12.45	—	6.60
NGC 6517	$10.60 \pm 1.06$	10.60	10.60	—	46.08	—	10.80
NGC 6522	$7.40 \pm 0.19$	7.70	8	7.40	14.35	7.40	7.80
NGC 6528	$7.70 \pm 0.77$	7.90	7.45	7.50	13.40	7.50	9.10
NGC 6535	$6.50 \pm 0.65$	6.80	6.50	—	7.73	—	6.70
NGC 6539	$7.85 \pm 0.66$	7.8	7.85	8.4	15.87	—	8.40
NGC 6540*	$5.20 \pm 0.52$	5.30	5.20	5.20	—	3.50	3.70
NGC 6541	$7.95 \pm 0.37$	7.5	7.95	—	8.78	—	7.00
NGC 6544	$3.0 \pm 0.30$	3.0	2.60	2.80	3.02	—	2.60
NGC 6553*	$6.75 \pm 0.22$	6.0	6.75	4.90	—	5.20	5.60
NGC 6558	$8.26 \pm 0.53$	7.40	7.20	—	—	8.26	7.40
NGC 6569	$10.59 \pm 0.80$	10.90	10.59	12.0	—	—	8.7
NGC 6624	$8.43 \pm 0.11$	7.9	7.19	8.4	7.26	8.32	8.00
NGC 6626	$5.34 \pm 0.17$	5.5	5.43	—	6.81	5.34	5.70
NGC 6637	$8.80 \pm 0.88$	8.80	8.80	9.40	13.40	8.85	8.60
NGC 6638*	$10.32 \pm 1.03$	9.40	10.32	13.5	—	—	8.40
NGC 6642	$8.10 \pm 0.81$	8.10	8.05	7.0	—	—	7.70
NGC 6652	$9.51 \pm 0.12$	10	10	6.8	9.09	9.44	9.60
NGC 6656	$3.20 \pm 0.32$	3.20	3.23	7.90	3.84	—	3.20
NGC 6681	$9.31 \pm 0.17$	9.0	9.31	—	9.12	—	—
NGC 6712	$6.95 \pm 0.39$	6.90	6.12	—	—	—	6.9
NGC 6717	$7.14 \pm 0.10$	7.10	7.10	—	8.0	7.15	7.40
NGC 6723	$8.17 \pm 0.11$	8.70	8.30	—	13.33	8.05	8.80
NGC 6752	$4.25 \pm 0.09$	4.0	4.25	—	4.32	4.36	4.0
NGC 6760	$7.95 \pm 0.50$	7.40	7.95	—	—	—	7.40
NGC 6809	$5.30 \pm 0.20$	5.40	5.30	—	5.86	—	5.40
NGC 6838	$4.0 \pm 0.20$	4.0	3.99	—	4.44	—	3.90
Palomar 11	$14.30 \pm 1.40$	13.4	14.30	—	—	—	12.9
Palomar 6*	$5.80 \pm 0.58$	5.80	5.80	—	—	8.90	7.30
Palomar 7	$5.39 \pm 0.51$	5.40	5.38	—	—	—	5.4
Palomar 8	$12.80 \pm 1.28$	12.80	12.80	—	—	—	12.9
Terzan 1	$6.70 \pm 0.67$	6.70	6.7	9.10	—	5.20	6.20
Terzan 10	$10.3 \pm 1.0$	5.8	5.8	6.6	—	10.30	5.70
Terzan 12	$3.40 \pm 0.34$	4.80	3.40	-	-	-	4.80
Terzan 2	$7.50 \pm 0.75$	7.50	7.50	8.20	—	7.70	8.70
Terzan 3	$8.20 \pm 0.82$	8.20	8.10	—	—	6.50	7.50
Terzan 4*	$6.70 \pm 0.67$	7.20	6.70	—	—	8.0	9.10
Terzan 5*	$5.50 \pm 0.51$	6.90	5.50	10.50	—	5.50	7.60
Terzan 6	$6.80 \pm 0.68$	6.80	6.70	6.0	—	7.0	9.50
Terzan 9*	$7.10 \pm 0.71$	7.10	7.10	11.60	—	4.90	7.70
Ton 2	$6.40 \pm 0.64$	8.20	6.40	—	—	6.40	8.10

\* GCs with the largest difference in distance determinations in the literature.

In the past, the measurement of absolute PMs was a difficult task, especially for GCs in the innermost Galaxy, and when available, the uncertainties were large, whereas now with Gaia that issue is essentially solved. Presently, the input distance values are the major source of uncertainty to construct more precise orbits along the Galaxy, and therefore, in the classification of the GCs into a specific stellar population. The distance values for some of them, in particular for the most reddened ones, can be significantly different from H10 or Baumgardt et al. (2019) with their kinematic distance estimations.

Table 2 shows a compilation of distances from the literature. The distances used for the orbital integration is given in column 2, the distance from H10 catalog is in column 3, the kinematics distances by Baumgardt et al. (2019) in column 4, distance determinations by Valenti et al. (2007, 2010) in column 5, the distance estimated by the inverse of the parallax from Gaia Collaboration et al. (2018b) is in column 6, distances taken from isochrone fittings of the CMD and RR Lyrae estimated by our group is given in column 7, and in column 8 is given the distance compilation by Bica et al. (2006).

The GCs with the largest difference in distance determinations in the literature are Djorg 1, Djorg 2, ESO452SC11, NGC 5927, NGC 6235, NGC 6256, NGC 6316, NGC 6380, NGC 6388, NGC 6401, NGC 6540, NGC 6553, NGC 6638, Palomar 6, Terzan 4, Terzan 5, and Terzan 9.

In order to have a reliable statistical estimate of the uncertainty in distances, we first compared distances from Bica et al. (2006) with those from Valenti et al. (2007, 2010) for 17 bulge clusters in common. These two samples are independent because the first is mostly optical-based and the other is near-infrared-based, with different reddening dependence and different isochrone sets. From the whole sample we have an uncertainty  $\sigma = 1.3$  kpc, but by removing two outliers with errors larger than 2 kpc, which clearly have some specific problems, the uncertainty goes down to  $\sigma = 0.99$  kpc. A second check comparing our adopted distances with respect to Baumgardt et al. (2019) and removing two outliers with differences larger than 4 kpc, this results in a standard deviation of 0.4 kpc. From these two comparisons, we adopt a mean standard deviation 0.7 kpc.

Note that Hilker et al. (2019) report an error on their proper motion distances of 8% at the distance of 7 kpc, which gives an error of 0.6 kpc at the typical distance of the bulge clusters of 7 kpc. This is very consistent with the suggested 0.7 kpc standard deviation.

### 3 THE GALACTIC POTENTIAL

In order to construct the orbits of the GCs, in this study we employ a non-axisymmetric model for the Galactic gravitational potential, that is built from an axisymmetric background that includes a Sérsic bulge, an exponential disc made by the superposition of three Miyamoto-Nagai potentials (Miyamoto & Nagai 1975), following the recipe given by Smith et al. (2015), and a Navarro-Frenk-White (NFW) density profile (Navarro et al. 1997) to model the dark matter halo, having a circular velocity  $V_0 = 241$  km s $^{-1}$  at  $R_0 = 8.2$  kpc (Bland-Hawthorn & Gerhard 2016). Even though the mass of the dark matter halo is twice larger than usual

**Table 3.** Parameters of the adopted Galactic mass model.

Parameter	Value	Reference
<b>Axisymmetric components</b>		
<b>Bulge</b>		
$M_{\mathrm{b},\mathrm{tot}}$	$1.2 \times 10^{10} M_{\odot}$	1, 2
$R_{\mathrm{e}}$	0.87 kpc	
$n$	1	3
<b>Disc</b>		
$M_{\mathrm{d},1}$	$1.07 \times 10^{11} M_{\odot}$	
$a_{\mathrm{d},1}$	5.97 kpc	
$M_{\mathrm{d},2}$	$-7.09 \times 10^{10} M_{\odot}$	
$a_{\mathrm{d},2}$	12.99 kpc	
$M_{\mathrm{d},3}$	$1.2 \times 10^{10} M_{\odot}$	
$a_{\mathrm{d},3}$	2.04 kpc	
$b_{\mathrm{d}}$	0.25 kpc	
<b>Halo</b>		
$M_{\mathrm{h}}$	$3.0 \times 10^{12} M_{\odot}$	4
$a_{\mathrm{h}}$	57.0 kpc	4
<b>Galactic bar</b>		
$M_{\mathrm{bar}}$	$1.2 \times 10^{10} M_{\odot}$	1, 2, 5
$n$	2	6
$a$	3.5 kpc	9, 10
$b$	1.4 kpc	9, 10
$c$	1.0 kpc	9, 10
$\phi_{\mathrm{bar}}$	25°	2, 7, 8
$\Omega_{\mathrm{bar}}$	40, 45, 50 km s $^{-1}$ kpc $^{-1}$	2, 11, 12, 13

**References.** (1) Portail et al. 2015a; (2) Bland-Hawthorn & Gerhard 2016; (3) Kent et al. 1991; (4) Irrgang et al. 2013; (5) Weiner & Sellwood 1999; (6) Pfenniger 1984; (7) Rattenbury et al. 2007; (8) Wegg & Gerhard 2013; (9) Freudenreich 1998; (10) Gardner & Flynn 2010; (11) Bissantz et al. 2003; (12) Portail et al. 2017; (13) Pérez-Villegas et al. 2017.

halo masses of  $1.0 - 1.5 \times 10^{12} M_{\odot}$ , with the scale radius we assumed, the rotation curve inside 30 kpc of our model is in agreement with Bland-Hawthorn & Gerhard (2016), as shown in Figure 3. We also adopted a less massive DM halo, also reducing the scale radius, and not significant differences are found.

For the Galactic bar, we used a triaxial Ferrer's ellipsoid, where all the mass from the bulge component is converted into a bar. For the bar potential, we consider a total bar mass of  $1.2 \times 10^{10} M_{\odot}$ , an angle of 25° with the Sun-major axis of the bar, a major axis extension of 3.5 kpc, and a gradient of the bar pattern speed values assumed to be  $\Omega_b = 40, 45$ , and 50 km s $^{-1}$  kpc $^{-1}$ . We keep the same bar extension in all cases, for any of the bar pattern speed values. Table 3 gives the parameters used for our Galactic model.

### 4 PROPERTIES OF THE GLOBULAR CLUSTER ORBITS

To construct the GC orbits through the Galactic potential, we have employed the Shampine–Gordon integration scheme that is implemented in the NIGO tool (Numerical Integrator of Galactic Orbits – Rossi 2015a).

We integrated the orbits for the present cluster sample forward in time for 10 Gyr. Using the observational

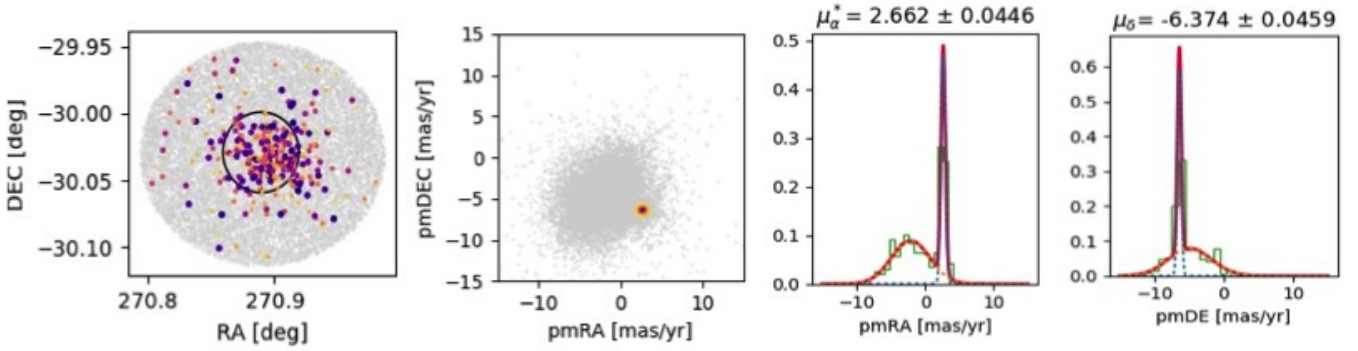


**Figure 2.** Example of proper motion data from Gaia DR2 for NGC 6522, and cluster member selection. First panel: core radius containing the field studied; second panel: location of the cluster in the vector-point diagram; third and fourth panels: Gaussian of RA and DEC proper motions respectively.

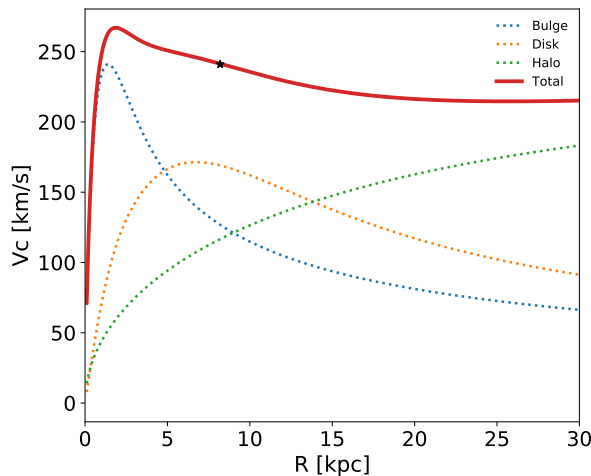


**Figure 3.** Total circular velocity curve and the contribution of each component of axisymmetric Galactic mass model. The black star shows the velocity at the Sun position.

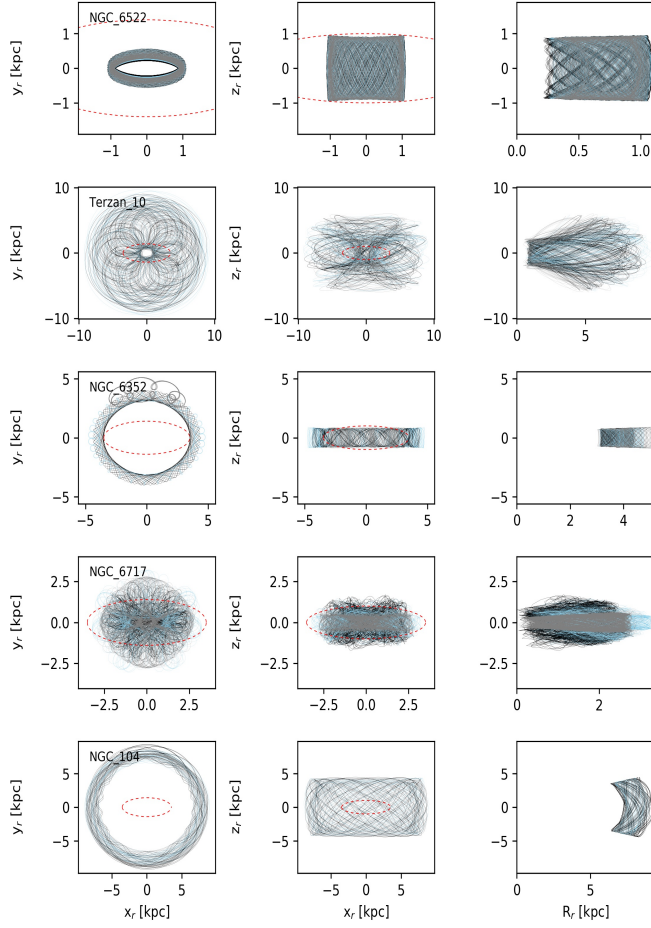
parameters of the GCs given in Table 1, we computed the initial state vector of the clusters assuming the Sun's Galactocentric distance  $R_0 = 8.2$  kpc and a circular velocity  $V_0 = 241$  km s $^{-1}$  (e.g. Bland-Hawthorn & Gerhard 2016, and references therein). The velocity components of the Sun with respect to the local standard of rest (LSR) are  $(U, V, W)_\odot = (11.1, 12.24, 7.25)$  km s $^{-1}$  (Schönrich et al. 2010). The velocity components of the cluster in the heliocentric reference system  $U, V$ , and  $W$  are positive in direction of the Galactic center, Galactic rotation, and North Galactic Pole, respectively. We defined as inertial Galactocentric frame of reference the right-handed system of coordinates  $(x, y, z)$  where the  $x$ -axis points to the Sun from the Galactic Centre and the  $z$ -axis points to the North Galactic Pole. We refer to the bar-corotating frame of reference as the right-handed system of coordinates  $(x_r, y_r, z_r)$  that co-rotates with

the bar, where the  $x_r$  axis is aligned with the bar semi-major axis  $a$  and  $z_r$  points towards the North Galactic Pole.

For each cluster we generate a set of 1000 initial conditions, where we follow the Monte Carlo technique taking into account the uncertainties on the heliocentric distance, PMs in both directions, and the radial velocity given in Table 1. The PM uncertainties include the average of the systematic error of 0.035 mas yr $^{-1}$  reported by the Gaia Collaboration et al. (2018b). These calculations were carried out with the purpose of evaluating how much the orbital properties of the GCs change due to the uncertainties of the observed data. Figure 4 shows some examples of orbits with the three different bar pattern speed values, in the frame co-rotating with the bar, for five GCs of our sample: NGC 6522, Terzan 10, NGC 6352, NGC 6717, and NGC 104 (from top to bottom). The initial conditions for them are the central values given in Table 1.

The orbital properties we calculate, in the inertial frame of reference, are the perigalactic distance  $r_{\min}$ , the apogalactic distance  $r_{\max}$ , the maximum vertical excursion from the Galactic plane  $|z|_{\max}$ , and the eccentricity defined as  $e = (r_{\max} - r_{\min})/(r_{\max} + r_{\min})$ .

In Table 4, we present the orbital parameters of our sample of GCs, where we use three values of rotational velocity of the bar  $\Omega_b = 40, 45$ , and 50 km s $^{-1}$  kpc $^{-1}$ . For each bar pattern speed, we give the average values of the perigalactic distance, apogalactic distance, the maximum vertical excursion from the Galactic plane, and the orbital eccentricity. The errors provided in each column are the standard deviation of the distribution. We see that for the clusters that are confined in the innermost Galaxy, such as HP 1, Djorg 2, Liller 1, and NGC 6325, the effect of the bar pattern speed is almost negligible. On the contrary, for NGC 5927, the perigalactic distance decreases with the pattern speed.



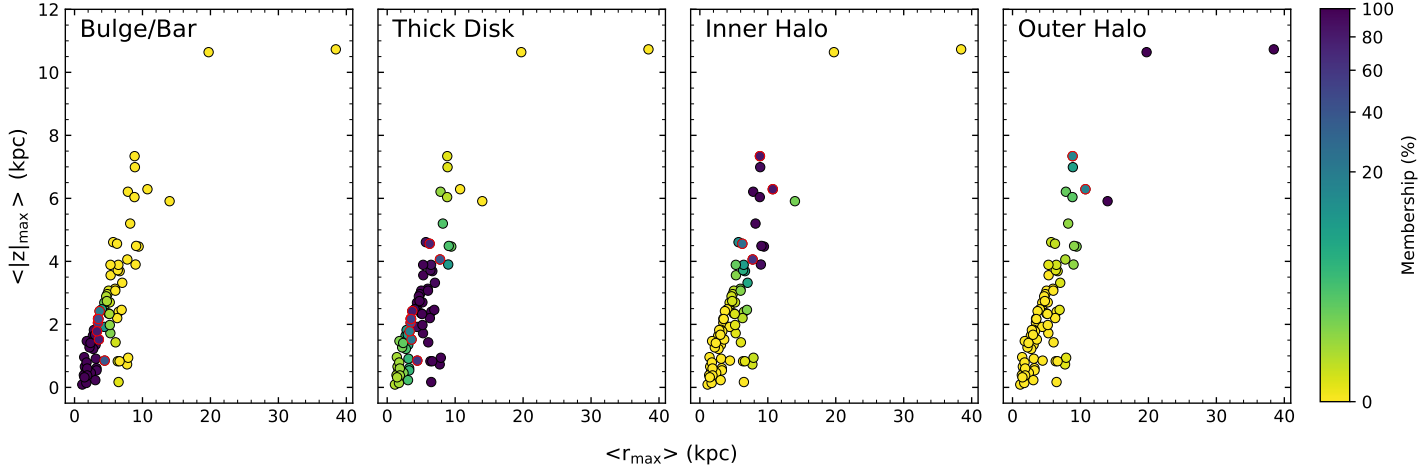
**Figure 4.** Examples of orbits for the globular clusters. The three columns show  $x - y$ ,  $x - z$ , and  $R - z$  projections for orbits with the non-axisymmetric Galactic potential co-rotating with the bar. The colors in the left panels are the orbits with different pattern speed of the bar, 40 (black), 45 (blue), and 50 (grey)  $\text{km s}^{-1} \text{kpc}^{-1}$ . The dashed red line shows the size of the Galactic bar.

Table 4: Orbital parameters for different bar pattern speed.

Cluster	$\Omega_b = 40 \text{ km s}^{-1} \text{kpc}^{-1}$	$\Omega_b = 45 \text{ km s}^{-1} \text{kpc}^{-1}$	$\Omega_b = 50 \text{ km s}^{-1} \text{kpc}^{-1}$	
	$\langle r_{\min} \rangle$ (kpc)	$\langle r_{\max} \rangle$ (kpc)	$\langle r_{\min} \rangle$ (kpc)	
BH 261	0.47 ± 0.60	3.10 ± 0.57	1.35 ± 0.17	0.74 ± 0.20
Djorg 1	0.52 ± 0.31	7.02 ± 2.42	3.32 ± 1.16	0.86 ± 0.05
Djorg 2	0.15 ± 0.12	1.67 ± 0.04	0.55 ± 0.09	0.83 ± 0.11
ESO452SC11	0.12 ± 0.16	3.45 ± 0.37	2.05 ± 0.12	0.93 ± 0.06
HP 1	0.12 ± 0.08	3.08 ± 0.37	1.83 ± 0.11	0.93 ± 0.04
Liller 1	0.08 ± 0.18	1.14 ± 0.41	0.09 ± 0.06	0.88 ± 0.23
Lynga 7	1.17 ± 0.74	5.27 ± 0.52	1.72 ± 0.25	0.62 ± 0.15
Mercer 5	1.83 ± 0.20	6.48 ± 1.19	0.17 ± 0.12	0.57 ± 0.06
NGC 104	7.22 ± 0.12	9.43 ± 0.98	4.47 ± 0.62	6.13 ± 0.05
NGC 5927	4.20 ± 0.21	6.36 ± 0.23	0.83 ± 0.03	0.21 ± 0.04
NGC 6139	0.27 ± 0.50	4.50 ± 0.76	2.63 ± 0.31	0.88 ± 0.14
NGC 6144	0.98 ± 0.69	5.69 ± 1.11	4.61 ± 0.63	0.71 ± 0.21
NGC 6171	0.58 ± 0.25	5.18 ± 0.42	2.70 ± 0.14	0.81 ± 0.08
NGC 6235	4.66 ± 1.70	19.73 ± 16.90	10.64 ± 9.66	0.61 ± 0.08
NGC 6256	2.00 ± 0.83	3.23 ± 0.38	0.61 ± 0.16	0.23 ± 0.22
NGC 6266	0.32 ± 0.14	2.75 ± 0.16	1.22 ± 0.17	0.80 ± 0.08
NGC 6273	0.19 ± 0.18	6.25 ± 0.92	4.56 ± 0.60	0.94 ± 0.06
NGC 6284	0.26 ± 0.94	8.84 ± 1.81	7.34 ± 1.56	0.94 ± 0.12
NGC 6287	0.18 ± 0.19	8.88 ± 2.06	6.99 ± 2.41	0.96 ± 0.03
NGC 6293	0.14 ± 0.10	4.38 ± 1.16	2.69 ± 0.64	0.94 ± 0.04
NGC 6304	0.96 ± 0.19	3.13 ± 0.16	0.91 ± 0.09	0.53 ± 0.07
NGC 6316	0.71 ± 0.86	4.98 ± 1.76	2.35 ± 0.49	0.76 ± 0.15
NGC 6325	0.14 ± 0.16	3.46 ± 0.91	2.18 ± 0.32	0.93 ± 0.08
NGC 6333	0.50 ± 0.23	10.73 ± 1.23	6.29 ± 1.46	0.91 ± 0.04
NGC 6342	0.14 ± 0.33	3.14 ± 0.68	1.77 ± 0.22	0.91 ± 0.11
NGC 6352	3.14 ± 0.30	4.43 ± 0.66	0.85 ± 0.06	0.19 ± 0.05
NGC 6355	0.14 ± 0.14	4.03 ± 1.19	2.48 ± 1.05	0.94 ± 0.05
NGC 6356	2.46 ± 2.18	9.06 ± 1.78	4.49 ± 1.13	0.58 ± 0.21
NGC 6362	2.94 ± 0.08	6.64 ± 0.11	3.69 ± 0.05	0.39 ± 0.02
NGC 6366	1.85 ± 0.29	6.49 ± 0.25	2.40 ± 0.16	0.56 ± 0.05
NGC 6380	0.13 ± 0.06	2.70 ± 0.92	1.64 ± 0.72	0.92 ± 0.06
NGC 6388	0.17 ± 0.09	5.96 ± 0.59	3.13 ± 0.65	0.94 ± 0.03
NGC 6401	0.13 ± 0.76	3.11 ± 0.24	1.64 ± 0.59	0.92 ± 0.09
NGC 6402	0.16 ± 0.16	5.01 ± 0.49	3.07 ± 0.19	0.94 ± 0.05
NGC 6440	0.09 ± 0.12	1.52 ± 0.41	0.66 ± 0.34	0.90 ± 0.11
NGC 6441	0.54 ± 0.23	4.38 ± 0.25	1.92 ± 0.36	0.78 ± 0.09
NGC 6453	0.24 ± 0.75	5.31 ± 1.79	3.56 ± 1.43	0.90 ± 0.13
NGC 6496	3.75 ± 1.32	13.99 ± 10.64	5.91 ± 5.49	0.60 ± 0.09
NGC 6517	0.14 ± 0.11	4.83 ± 0.70	2.96 ± 0.40	0.94 ± 0.03
NGC 6522	0.23 ± 0.11	1.42 ± 0.10	0.96 ± 0.02	0.72 ± 0.11
NGC 6528	0.07 ± 0.04	1.77 ± 0.49	0.79 ± 0.27	0.92 ± 0.03
NGC 6535	0.26 ± 0.40	7.77 ± 1.20	4.06 ± 0.89	0.94 ± 0.13
NGC 6539	1.56 ± 0.46	3.69 ± 0.58	2.42 ± 0.38	0.38 ± 0.14
NGC 6540	0.78 ± 0.52	3.24 ± 0.50	0.54 ± 0.16	0.61 ± 0.13
NGC 6541	0.90 ± 0.36	6.00 ± 0.47	3.07 ± 0.25	0.75 ± 0.10

**Table 4 – continued**

Cluster	$\langle r_{\min} \rangle$ (kpc)	$\langle r_{\max} \rangle$ (kpc)	$\langle z_{\max} \rangle$ (kpc)	$\langle e \rangle$	$\langle r_{\min} \rangle$ (kpc)	$\langle r_{\max} \rangle$ (kpc)	$\langle z_{\max} \rangle$ (kpc)	$\langle e \rangle$	$\langle r_{\min} \rangle$ (kpc)	$\langle r_{\max} \rangle$ (kpc)	$\langle z_{\max} \rangle$ (kpc)	$\langle e \rangle$
NGC 6544	0.17 ± 0.14	6.36 ± 0.53	3.72 ± 0.86	0.95 ± 0.04	0.19 ± 0.14	7.12 ± 0.76	3.75 ± 0.83	0.95 ± 0.04	0.17 ± 0.14	6.37 ± 0.57	3.38 ± 0.65	0.95 ± 0.04
NGC 6553	0.20 ± 0.09	2.40 ± 0.17	0.46 ± 0.03	0.85 ± 0.05	0.29 ± 0.09	2.36 ± 0.17	0.45 ± 0.04	0.78 ± 0.05	0.26 ± 0.14	2.29 ± 0.16	0.44 ± 0.02	0.79 ± 0.07
NGC 6558	0.10 ± 0.07	2.20 ± 0.31	1.27 ± 0.23	0.92 ± 0.05	0.10 ± 0.06	2.19 ± 0.30	1.29 ± 0.23	0.91 ± 0.05	0.09 ± 0.07	2.17 ± 0.33	1.32 ± 0.23	0.92 ± 0.05
NGC 6569	0.42 ± 1.01	3.58 ± 1.12	1.52 ± 0.21	0.79 ± 0.25	0.63 ± 0.91	3.78 ± 1.22	1.48 ± 0.20	0.72 ± 0.21	0.59 ± 0.87	3.71 ± 1.36	1.42 ± 0.19	0.73 ± 0.18
NGC 6624	0.08 ± 0.03	1.80 ± 0.26	1.47 ± 0.04	0.92 ± 0.03	0.08 ± 0.03	1.84 ± 0.18	1.46 ± 0.03	0.92 ± 0.03	0.08 ± 0.03	1.77 ± 0.11	1.46 ± 0.04	0.92 ± 0.03
NGC 6626	0.14 ± 0.09	3.30 ± 0.21	1.78 ± 0.22	0.92 ± 0.05	0.14 ± 0.13	3.32 ± 0.27	1.72 ± 0.19	0.92 ± 0.06	0.13 ± 0.10	3.36 ± 0.33	1.69 ± 0.25	0.92 ± 0.05
NGC 6637	0.12 ± 0.39	2.85 ± 0.72	1.82 ± 0.25	0.92 ± 0.14	0.11 ± 0.44	2.82 ± 0.73	1.82 ± 0.24	0.92 ± 0.17	0.11 ± 0.44	2.87 ± 0.81	1.79 ± 0.25	0.92 ± 0.16
NGC 6638	0.12 ± 0.09	3.51 ± 0.97	2.17 ± 0.48	0.93 ± 0.03	0.11 ± 0.10	3.59 ± 1.05	2.16 ± 0.48	0.94 ± 0.03	0.11 ± 0.10	3.78 ± 1.09	2.13 ± 0.46	0.94 ± 0.03
NGC 6642	0.10 ± 0.09	2.35 ± 0.48	1.41 ± 0.38	0.92 ± 0.06	0.10 ± 0.11	2.24 ± 0.52	1.38 ± 0.41	0.92 ± 0.06	0.09 ± 0.10	2.30 ± 0.58	1.43 ± 0.42	0.93 ± 0.06
NGC 6652	0.13 ± 0.08	4.66 ± 0.54	2.89 ± 0.13	0.94 ± 0.03	0.13 ± 0.10	4.72 ± 0.56	2.91 ± 0.15	0.94 ± 0.04	0.16 ± 0.11	4.82 ± 0.88	2.96 ± 0.17	0.94 ± 0.04
NGC 6656	4.35 ± 0.28	38.45 ± 4.75	10.73 ± 5.56	0.80 ± 0.03	0.43 ± 0.29	38.37 ± 4.76	11.06 ± 5.48	0.80 ± 0.03	4.32 ± 0.28	38.59 ± 4.75	10.72 ± 5.52	0.80 ± 0.03
NGC 6681	0.16 ± 0.07	7.85 ± 0.62	6.21 ± 0.44	0.96 ± 0.02	0.15 ± 0.07	7.99 ± 0.99	6.43 ± 0.48	0.96 ± 0.02	0.16 ± 0.09	8.56 ± 1.03	6.41 ± 0.75	0.96 ± 0.02
NGC 6712	0.37 ± 0.19	6.45 ± 0.86	3.89 ± 0.36	0.90 ± 0.05	0.53 ± 0.25	7.42 ± 0.66	3.61 ± 0.30	0.87 ± 0.06	0.54 ± 0.27	5.94 ± 0.34	2.90 ± 0.50	0.83 ± 0.08
NGC 6717	0.13 ± 0.11	3.02 ± 0.21	1.67 ± 0.14	0.92 ± 0.06	0.27 ± 0.18	3.32 ± 0.23	1.45 ± 0.13	0.85 ± 0.08	0.18 ± 0.15	3.16 ± 0.23	1.46 ± 0.11	0.89 ± 0.07
NGC 6723	0.52 ± 0.32	5.29 ± 0.61	3.89 ± 0.14	0.84 ± 0.10	0.57 ± 0.35	4.82 ± 0.93	3.92 ± 0.16	0.81 ± 0.13	0.23 ± 0.30	4.73 ± 0.95	3.90 ± 0.18	0.91 ± 0.11
NGC 6752	3.25 ± 0.11	6.93 ± 0.12	2.46 ± 0.07	0.36 ± 0.02	0.25 ± 0.14	6.51 ± 0.15	2.34 ± 0.05	0.44 ± 0.03	3.52 ± 0.20	6.38 ± 0.09	2.33 ± 0.05	0.29 ± 0.03
NGC 6760	1.62 ± 0.25	6.04 ± 0.22	1.43 ± 0.57	0.58 ± 0.06	1.51 ± 0.19	6.11 ± 0.53	1.05 ± 0.46	0.60 ± 0.05	1.14 ± 0.22	7.28 ± 0.32	1.10 ± 0.38	0.73 ± 0.05
NGC 6809	0.92 ± 0.24	8.19 ± 0.79	5.20 ± 0.30	0.80 ± 0.05	0.72 ± 0.38	7.62 ± 1.02	4.94 ± 0.29	0.84 ± 0.07	1.05 ± 0.21	8.74 ± 1.12	4.97 ± 0.35	0.78 ± 0.05
NGC 6838	4.75 ± 0.86	7.73 ± 0.14	0.73 ± 0.08	0.24 ± 0.10	4.75 ± 0.69	7.60 ± 0.14	0.72 ± 0.06	0.23 ± 0.07	4.73 ± 0.67	7.68 ± 0.23	0.73 ± 0.06	0.24 ± 0.06
Palomar 11	5.57 ± 2.53	8.98 ± 1.59	3.90 ± 0.62	0.23 ± 0.16	5.67 ± 2.55	8.99 ± 1.56	3.92 ± 0.62	0.25 ± 0.17	5.62 ± 2.49	9.60 ± 1.53	4.12 ± 0.60	0.26 ± 0.17
Palomar 6	0.17 ± 0.20	4.76 ± 1.06	2.74 ± 0.55	0.93 ± 0.06	0.15 ± 0.21	4.71 ± 1.22	2.71 ± 0.55	0.93 ± 0.05	0.17 ± 0.24	4.77 ± 1.53	2.67 ± 0.56	0.93 ± 0.06
Palomar 7	2.86 ± 0.33	7.89 ± 0.90	0.94 ± 0.07	0.47 ± 0.06	2.61 ± 0.62	7.36 ± 0.48	0.88 ± 0.05	0.45 ± 0.07	3.46 ± 0.61	7.10 ± 0.61	0.84 ± 0.05	0.35 ± 0.07
Palomar 8	2.01 ± 1.67	6.28 ± 1.27	2.20 ± 0.21	0.51 ± 0.22	2.03 ± 1.66	6.55 ± 1.21	2.16 ± 0.24	0.55 ± 0.22	1.82 ± 1.67	6.31 ± 1.15	2.22 ± 0.25	0.55 ± 0.22
Terzan 1	0.05 ± 0.05	1.73 ± 0.64	0.14 ± 0.01	0.95 ± 0.06	0.05 ± 0.08	1.70 ± 0.65	0.14 ± 0.02	0.94 ± 0.07	0.04 ± 0.08	1.72 ± 0.66	0.14 ± 0.02	0.95 ± 0.07
Terzan 10	0.57 ± 0.71	8.82 ± 5.04	6.04 ± 4.77	0.87 ± 0.06	0.60 ± 0.71	9.85 ± 5.11	6.11 ± 4.89	0.87 ± 0.06	0.59 ± 0.70	9.43 ± 5.11	6.32 ± 4.83	0.87 ± 0.06
Terzan 12	2.64 ± 0.44	6.63 ± 0.82	0.83 ± 0.09	0.43 ± 0.04	2.19 ± 0.75	7.42 ± 0.65	0.87 ± 0.09	0.46 ± 0.09	3.29 ± 0.78	7.10 ± 0.42	0.85 ± 0.11	0.37 ± 0.10
Terzan 2	0.05 ± 0.03	1.37 ± 0.54	0.39 ± 0.23	0.94 ± 0.03	0.05 ± 0.03	1.35 ± 0.56	0.38 ± 0.23	0.93 ± 0.03	0.06 ± 0.04	1.36 ± 0.57	0.38 ± 0.12	0.93 ± 0.06
Terzan 3	1.32 ± 0.62	5.13 ± 0.61	2.33 ± 0.52	0.62 ± 0.16	1.71 ± 0.35	5.77 ± 0.67	2.21 ± 0.59	0.56 ± 0.09	1.77 ± 0.36	6.18 ± 0.42	2.43 ± 0.46	0.54 ± 0.09
Terzan 4	0.09 ± 0.13	1.86 ± 0.57	0.60 ± 0.15	0.91 ± 0.09	0.11 ± 0.12	1.87 ± 0.57	0.59 ± 0.14	0.89 ± 0.06	0.09 ± 0.15	1.89 ± 0.60	0.59 ± 0.13	0.90 ± 0.07
Terzan 5	0.47 ± 0.26	3.06 ± 0.55	0.23 ± 0.06	0.72 ± 0.06	0.48 ± 0.21	3.04 ± 0.57	0.23 ± 0.06	0.71 ± 0.05	0.54 ± 0.23	3.14 ± 0.61	0.24 ± 0.11	0.70 ± 0.06
Terzan 6	0.06 ± 0.03	1.86 ± 0.72	0.38 ± 0.51	0.94 ± 0.03	0.06 ± 0.03	1.84 ± 0.76	0.39 ± 0.46	0.94 ± 0.03	0.05 ± 0.03	1.83 ± 0.73	0.38 ± 0.46	0.95 ± 0.03
Terzan 9	0.11 ± 0.05	1.46 ± 0.47	0.32 ± 0.06	0.87 ± 0.07	0.10 ± 0.04	1.46 ± 0.47	0.33 ± 0.05	0.88 ± 0.08	0.12 ± 0.06	1.47 ± 0.46	0.33 ± 0.08	0.84 ± 0.09
Ton 2	1.39 ± 0.68	5.19 ± 0.85	1.98 ± 0.18	0.57 ± 0.14	1.75 ± 0.59	5.74 ± 0.85	1.92 ± 0.18	0.54 ± 0.10	1.88 ± 0.48	5.93 ± 0.59	1.91 ± 0.19	0.54 ± 0.10



**Figure 5.** Membership probability for  $\Omega_b = 40 \text{ km s}^{-1} \text{ kpc}^{-1}$ . From left to right panel shows the probability that each GC has to belong to the bulge/bar, thick disk, inner halo, and outer halo, respectively. Open red circles highlight the clusters with probabilities between 15% to 85% that are in the boundary of two Galactic component.

Table 5: Membership probability for different bar pattern speed.

Cluster	$\Omega_b = 40 \text{ km s}^{-1} \text{ kpc}^{-1}$				$\Omega_b = 45 \text{ km s}^{-1} \text{ kpc}^{-1}$				$\Omega_b = 50 \text{ km s}^{-1} \text{ kpc}^{-1}$			
	Bulge	Disk thick	Halo inner %	Halo outer	Bulge	Disk thick	Halo inner %	Halo outer	Bulge	Disk thick	Halo inner %	Halo outer
BH 261	94.2	5.8	0.0	0.0	93.4	6.6	0.0	0.0	93.4	6.6	0.0	0.0
Djorg 1	0.0	93.4	6.6	0.0	0.0	88.7	11.3	0.0	0.0	93.2	6.8	0.0
Djorg 2	99.8	0.2	0.0	0.0	99.8	0.2	0.0	0.0	99.7	0.3	0.0	0.0
ESO452SC11	59.2	40.8	0.0	0.0	59.6	40.4	0.0	0.0	54.3	45.7	0.0	0.0
HP 1	86.5	13.5	0.0	0.0	85.4	14.6	0.0	0.0	87.6	12.4	0.0	0.0
Liller 1	99.8	0.2	0.0	0.0	99.8	0.2	0.0	0.0	99.8	0.2	0.0	0.0
Lynga 7	0.7	99.3	0.0	0.0	0.3	99.7	0.0	0.0	0.0	100.0	0.0	0.0
Mercer 5	0.0	100.0	0.0	0.0	0.0	100.0	0.0	0.0	0.0	100.0	0.0	0.0
NGC 104	0.0	1.2	98.0	0.8	0.0	2.3	97.1	0.6	0.0	3.5	96.0	0.5
NGC 5927	0.0	100.0	0.0	0.0	0.1	99.9	0.0	0.0	0.1	99.9	0.0	0.0
NGC 6139	0.8	99.2	0.0	0.0	0.5	99.4	0.0	0.0	0.8	99.1	0.0	0.0
NGC 6144	0.0	87.1	12.9	0.1	0.0	74.3	25.6	0.1	0.0	71.2	28.7	0.1
NGC 6171	0.0	99.9	0.1	0.0	0.1	99.9	0.1	0.0	0.1	99.9	0.0	0.0
NGC 6235	0.0	0.0	0.0	100.0	0.0	0.0	0.0	100.0	0.0	0.0	0.0	100.0
NGC 6256	96.0	4.0	0.0	0.0	95.9	4.1	0.0	0.0	94.5	5.5	0.0	0.0
NGC 6266	97.7	2.3	0.0	0.0	97.7	2.3	0.0	0.0	97.2	2.8	0.0	0.0
NGC 6273	0.0	73.9	26.1	0.1	0.0	80.3	19.6	0.1	0.0	55.5	44.3	0.1
NGC 6284	0.0	0.0	83.8	16.1	0.0	0.0	46.7	53.3	0.0	0.0	65.4	34.6
NGC 6287	0.0	0.0	91.7	8.3	0.0	0.0	74.7	25.3	0.0	0.0	58.8	41.2
NGC 6293	1.1	98.9	0.0	0.0	1.7	98.2	0.0	0.0	2.0	98.0	0.0	0.0
NGC 6304	96.3	3.7	0.0	0.0	96.0	4.0	0.0	0.0	94.7	5.3	0.0	0.0
NGC 6316	0.4	99.6	0.0	0.0	0.4	99.6	0.0	0.0	0.4	99.6	0.0	0.0
NGC 6325	49.3	50.7	0.0	0.0	43.3	56.7	0.0	0.0	44.7	55.3	0.0	0.0
NGC 6333	0.0	0.0	82.9	17.1	0.0	0.0	64.9	35.1	0.0	0.0	47.8	52.2
NGC 6342	86.6	13.4	0.0	0.0	83.7	16.3	0.0	0.0	82.7	17.3	0.0	0.0
NGC 6352	38.3	61.7	0.0	0.0	11.7	88.3	0.0	0.0	2.8	97.2	0.0	0.0
NGC 6355	6.7	93.3	0.0	0.0	4.1	95.9	0.0	0.0	2.6	97.4	0.0	0.0
NGC 6356	0.0	2.3	97.2	0.6	0.0	3.6	96.0	0.4	0.0	2.8	96.7	0.5
NGC 6362	0.0	91.9	8.1	0.0	0.0	99.5	0.5	0.0	0.0	99.6	0.4	0.0
NGC 6366	0.0	99.7	0.3	0.0	0.0	98.5	1.5	0.0	0.0	99.5	0.5	0.0
NGC 6380	95.8	4.2	0.0	0.0	95.4	4.6	0.0	0.0	94.1	5.9	0.0	0.0
NGC 6388	0.0	99.3	0.7	0.0	0.0	93.9	6.0	0.0	2.1	97.9	0.0	0.0
NGC 6401	90.3	9.7	0.0	0.0	90.1	9.9	0.0	0.0	90.5	9.5	0.0	0.0
NGC 6402	0.0	99.9	0.1	0.0	0.0	99.9	0.1	0.0	0.0	99.9	0.1	0.0
NGC 6440	99.8	0.2	0.0	0.0	99.8	0.2	0.0	0.0	99.8	0.2	0.0	0.0
NGC 6441	11.0	89.0	0.0	0.0	7.0	93.0	0.0	0.0	8.8	91.2	0.0	0.0
NGC 6453	0.0	99.4	0.6	0.0	0.0	99.4	0.6	0.0	0.0	95.2	4.8	0.0

**Table 5 – continued**

Cluster	Bulge	Disk thick	Halo inner %	Halo outer	Bulge	Disk thick	Halo inner %	Halo outer	Bulge	Disk thick	Halo inner %	Halo outer
NGC 6496	0.0	0.0	0.9	99.1	0.0	0.0	9.4	90.6	0.0	0.0	14.7	85.3
NGC 6517	0.1	99.9	0.1	0.0	0.1	99.9	0.1	0.0	0.1	99.8	0.0	0.0
NGC 6522	99.8	0.2	0.0	0.0	99.8	0.2	0.0	0.0	99.8	0.2	0.0	0.0
NGC 6528	99.7	0.3	0.0	0.0	99.7	0.3	0.0	0.0	99.7	0.3	0.0	0.0
NGC 6535	0.0	38.9	60.9	0.2	0.0	99.9	0.1	0.0	0.0	99.9	0.1	0.0
NGC 6539	19.5	80.5	0.0	0.0	2.2	97.8	0.0	0.0	0.5	99.5	0.0	0.0
NGC 6540	96.1	3.9	0.0	0.0	95.9	4.1	0.0	0.0	95.8	4.2	0.0	0.0
NGC 6541	0.0	99.4	0.6	0.0	0.0	98.6	1.4	0.0	0.0	94.2	5.7	0.0
NGC 6544	0.0	94.6	5.4	0.0	0.0	80.7	19.3	0.1	0.0	97.4	2.6	0.0
NGC 6553	99.3	0.7	0.0	0.0	99.4	0.6	0.0	0.0	99.4	0.6	0.0	0.0
NGC 6558	99.1	0.9	0.0	0.0	99.1	0.9	0.0	0.0	99.1	0.9	0.0	0.0
NGC 6569	78.0	22.0	0.0	0.0	68.5	31.5	0.0	0.0	74.6	25.4	0.0	0.0
NGC 6624	99.3	0.7	0.0	0.0	99.3	0.7	0.0	0.0	99.3	0.7	0.0	0.0
NGC 6626	81.1	18.9	0.0	0.0	82.4	17.6	0.0	0.0	81.8	18.2	0.0	0.0
NGC 6637	91.7	8.3	0.0	0.0	92.2	7.8	0.0	0.0	91.8	8.2	0.0	0.0
NGC 6638	46.7	53.3	0.0	0.0	42.3	57.7	0.0	0.0	32.1	67.9	0.0	0.0
NGC 6642	98.5	1.5	0.0	0.0	98.8	1.2	0.0	0.0	98.6	1.4	0.0	0.0
NGC 6652	0.2	99.8	0.0	0.0	0.1	99.8	0.0	0.0	0.1	99.9	0.1	0.0
NGC 6656	0.0	0.0	0.0	100.0	0.0	0.0	0.0	100.0	0.0	0.0	0.0	100.0
NGC 6681	0.0	0.4	98.3	1.3	0.0	0.2	97.9	1.9	0.0	0.1	97.5	2.4
NGC 6712	0.0	90.8	9.2	0.0	0.0	77.7	22.2	0.1	0.0	99.6	0.4	0.0
NGC 6717	91.4	8.6	0.0	0.0	88.9	11.1	0.0	0.0	92.1	7.9	0.0	0.0
NGC 6723	0.0	98.6	1.4	0.0	0.0	99.4	0.6	0.0	0.0	99.5	0.5	0.0
NGC 6752	0.0	99.3	0.7	0.0	0.0	99.8	0.2	0.0	0.0	99.8	0.2	0.0
NGC 6760	0.0	100.0	0.0	0.0	0.0	99.9	0.0	0.0	0.0	100.0	0.0	0.0
NGC 6809	0.0	2.1	97.4	0.5	0.0	9.6	90.1	0.3	0.0	1.3	98.1	0.5
NGC 6838	0.0	100.0	0.0	0.0	0.0	100.0	0.0	0.0	0.0	100.0	0.0	0.0
Palomar 11	0.0	9.6	89.9	0.5	0.0	9.1	90.4	0.5	0.0	2.0	97.1	0.9
Palomar 6	0.2	99.8	0.0	0.0	0.3	99.7	0.0	0.0	0.3	99.7	0.0	0.0
Palomar 7	0.0	99.9	0.1	0.0	0.0	100.0	0.0	0.0	0.0	100.0	0.0	0.0
Palomar 8	0.0	99.9	0.1	0.0	0.0	99.8	0.2	0.0	0.0	99.9	0.1	0.0
Terzan 1	99.7	0.3	0.0	0.0	99.7	0.3	0.0	0.0	99.7	0.3	0.0	0.0
Terzan 10	0.0	0.1	98.2	1.7	0.0	0.0	95.3	4.7	0.0	0.0	95.9	4.1
Terzan 12	0.0	100.0	0.0	0.0	0.0	100.0	0.0	0.0	0.0	100.0	0.0	0.0
Terzan 2	99.8	0.2	0.0	0.0	99.8	0.2	0.0	0.0	99.8	0.2	0.0	0.0
Terzan 3	0.2	99.8	0.0	0.0	0.0	99.9	0.0	0.0	0.0	99.8	0.2	0.0
Terzan 4	99.7	0.3	0.0	0.0	99.7	0.3	0.0	0.0	99.7	0.3	0.0	0.0
Terzan 5	97.4	2.6	0.0	0.0	97.5	2.5	0.0	0.0	96.9	3.1	0.0	0.0
Terzan 6	99.7	0.3	0.0	0.0	99.7	0.3	0.0	0.0	99.7	0.3	0.0	0.0
Terzan 9	99.8	0.2	0.0	0.0	99.8	0.2	0.0	0.0	99.8	0.2	0.0	0.0
Ton 2	0.5	99.5	0.0	0.0	0.1	99.9	0.0	0.0	0.0	99.9	0.0	0.0

## 5 CLASSIFYING GLOBULAR CLUSTERS

In the literature, GCs have been classified based on their spatial distribution, metallicity, and internal and structural parameters (e.g. Aguilar et al. 1988; Minniti 1995; Barbuy et al. 1998; Côté 1999; Bica et al. 2016; Pasquato & Chung 2019). In this section, we used the orbital parameters of the 78 GCs, calculated in Section 4, to separate the clusters into different stellar populations. We obtained this classification using unsupervised clustering algorithms.

### 5.1 Clustering method

The identification of GCs that are confined or belong to the bulge/bar component, which is the main aim of the present work, is not an easy task because in the innermost part of the Galaxy, all components overlap: the bulge/bar, thick disk, inner halo, and outer halo.

In terms of dynamics, the GCs of each component should share its dynamical properties. Based on this criterion, we employed the orbital parameters (Table 4) to separate the GCs into four Galactic components: bulge/bar, thick disk, inner halo, and outer halo. To do this classification, we employ the Gaussian Mixture Models (GMM), an unsupervised machine learning algorithm that searches for  $K$  Gaussian distributions, which fits better a  $ND$  parameter space. Based on Bayes's theorem, the GMM algorithm tries to maximize the expression:

$$G(x) = \sum_{i=1}^K \phi_i \times N(x|\mu_i, \sigma_i),$$

where  $N(x|\mu_i, \sigma_i)$  represents the  $i$ th Gaussian distribution with mean  $\mu_i$  and standard deviation  $\sigma_i$ . The  $\vec{x}$  is the parameter space.

We employed the 2D GMM clustering algorithm using two orbital parameters: the apogalactic distance  $r_{max}$  and the maximum height from the plane  $|z|_{max}$ . For the GCs separation, we take into account the contribution of the set of orbits of each GC and the three bar pattern speeds. To prevent confusion in the clustering method, we removed the orbits with  $r_{max} > 20$  kpc.

From the GMM algorithm, we obtain the centre  $\mu_i(r_{max}, |z|_{max})$ , width  $\sigma_i(r_{max}, |z|_{max})$ , and weight  $P_i$  of each stellar component. For the bulge/bar component  $\mu_b = (2.50, 1.07)$  kpc,  $\sigma_b = (0.83, 0.63)$  kpc, and  $P_b = 0.38$ ; for the thick disk  $\mu_d = (5.60, 2.42)$  kpc,  $\sigma_d = (1.29, 1.09)$  kpc, and  $P_d = 0.46$ ; for the inner halo  $\mu_{H_i} = (8.60, 5.12)$  kpc,  $\sigma_{H_i} = (1.31, 1.02)$  kpc, and  $P_{H_i} = 0.11$ , and outer halo  $\mu_{H_o} = (12.75, 8.47)$  kpc,  $\sigma_{H_o} = (2.57, 2.18)$  kpc, and  $P_{H_o} = 0.032$ .

For the present work, a statistical approach was necessary since the classification depends on the distribution of the data in the parameter space and their uncertainties. The GMM was applied from the library `scikit-learn` (Pedregosa et al. 2011).

### 5.2 Membership probability and GC classification

With the information of the each component provided by the GMM and using a Gaussian distribution probability, we calculate the membership probability that each cluster has to belong to each Galactic component. Figure 5 shows the

membership probability for  $\Omega_b = 40 \text{ km s}^{-1} \text{ kpc}^{-1}$ . The dark blue color indicates the clusters that have probability higher than 85% to belong to the bulge/bar (first panel), thick disk (second panel), inner halo (third panel), and outer halo (four panel) component. The red open circles mark the clusters with probability between 15% to 85%, those clusters are in the boundary between two Galactic components. Table 5 gives the probability for each cluster to be part of the bulge, disk, inner halo, and outer halo, for the three pattern speeds of the bar.

The maximum probability of membership given in Table 5 was used to classify the GCs into each Galactic component. Figure 6 shows a plot of combinations among the orbital parameters, where the colours identify the groups of clusters based on the membership probability. Figure 6 also shows a clear correlation between  $\langle r_{max} \rangle$  and  $\langle |z|_{max} \rangle$ , and an anticorrelation between  $\langle r_{min} \rangle$  and eccentricity.

In Table 6, we list the GCs that belong to each of the Galactic components. Our sample has 40 out of 43 GCs identified as bulge GCs in Bica et al. (2016), and based on their dynamical properties, for the pattern speed of  $40 \text{ km s}^{-1} \text{ kpc}^{-1}$ , we found that 27 of them, have characteristics of bulge GCs with a higher probability, whereas the other 13 GCs (Mercer 5, NGC 6316, NGC 6325, NGC 6355, NGC 6539, NGC 6638, NGC 6652, Ton 2, Palomar 6, Djorg 1, Terzan 3, Terzan 10, and NGC 6723) appear to be intruders from other stellar components, that currently are crossing the central parts of the Galaxy, provided that their distances are confirmed in the future. Additionally, the cluster NGC 6380 and NGC 6569 are part of the bulge GCs in our classification, therefore we have 29 bulge GCs. Another 37, 9, and 3 GCs are identified as thick disk, inner halo, and outer halo, respectively. There are three clusters, NGC 6535, NGC 6284, and NGC 6333, that change of component with the bar pattern speed. Additionally, there are clusters with significant probability to be in two stellar components. ESO452SC11, NGC 6325, NGC 6352, NGC 6539, NGC 6569, NGC 6626, and NGC 6638 are in the boundary between bulge/bar and thick disk; NGC 6273 and NGC 6535 are between thick disk and inner halo; NGC 6284 and NGC 6333 are between inner halo and outer halo, and those clusters could change with the bar pattern speed. It is important to stress that due to the uncertainties of the data, in particular in the distances, the classification established here, might change in the future when better distance determinations are available. One example is Palomar 6, that with the distance of  $d_\odot = 5.8$  kpc puts it in the thick disk component whereas with the distance by Ortolani et al. (1995) of  $d_\odot = 8.9$  kpc puts it in the bulge.

Figure 7 shows the spatial distribution of the sample GCs, based on our classification and the stellar component with higher membership probability, where we can note that GCs from different Galactic components overlap in the innermost part of the Galaxy.

## 6 BULGE GLOBULAR CLUSTERS

Once we identify clusters with high probability to be bulge GCs, we analyze their set of orbits, with the purpose of knowing which bulge GCs follow the bar. To classify orbits, we use the same criteria as Portail et al. (2015b). The orbit

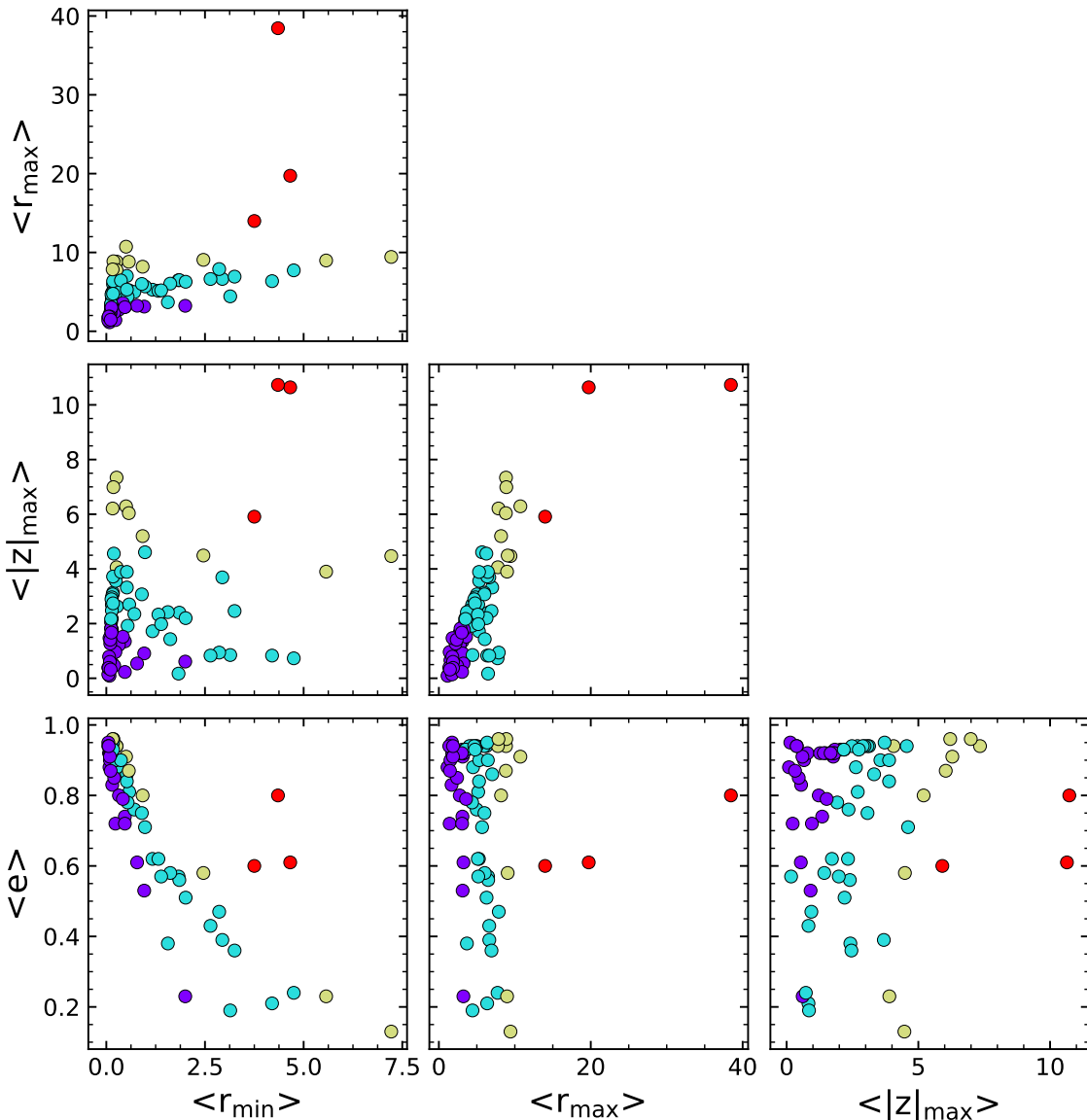


**Figure 6.** Orbital parameters as function of the median value of the perigalactic distance  $\langle r_{min} \rangle$ , the apogalactic distance  $\langle r_{max} \rangle$ , and the maximum distance from the Galactic plane  $\langle |z|_{max} \rangle$ , for  $\Omega_b = 40 \text{ km s}^{-1} \text{ kpc}^{-1}$ . The four groups are: bulge/bar (purple), thick disk (cyan), inner halo (green), and outer halo (red).

classification employs frequency analysis. First, we compute the fast Fourier transform for each orbit in the Cartesian  $x$  coordinate and the Cylindrical radius  $R$ , to identify the main frequencies. Then, the orbits for which the frequency ratio  $f_R/f_x = 2 \pm 0.1$  are bar-following orbits. The orbits that are not supporting the bar-shape have a frequency ratio  $f_R/f_x \neq 2 \pm 0.1$ . Table 7 gives the percentage of orbits in each bulge GC that support the bar shape. The clusters Liller 1, NGC 6304, NGC 6522, NGC 6528, NGC 6540, NGC 6553, Terzan 5, and Terzan 9 have more than 20% of their orbits that support the bar. The fraction of orbits that follow the Galactic bar decreases with the rotation of the bar, except for the cases of NGC 6304, NGC 6342, and NGC 6637, that increases instead. Also, we found that most of the bulge/bar GCs are not supporting the Galactic bar.

On the other hand, there are bulge GCs that even if they are not supporting the bar shape, they are trapped into a bar resonance such as NGC 6266 and NGC 6558, in the 3:1 resonance.

Additionally, the metallicity distribution function (MDF) of the classified bulge GCs is shown in Figure 8, where we can note a clear peak at  $[\text{Fe}/\text{H}] \sim -1.0$ , as previously already reported by Rossi et al. (2015b) and Bica et al. (2016). Figure 9 gives the metallicity as a function of the orbital parameters, the perigalactic and apogalactic distances, the maximum height, and the eccentricity. We cannot see any trend among orbital parameters with the metallicity. Also, the effect of changing the bar pattern speed is almost negligible for the bulge GCs.

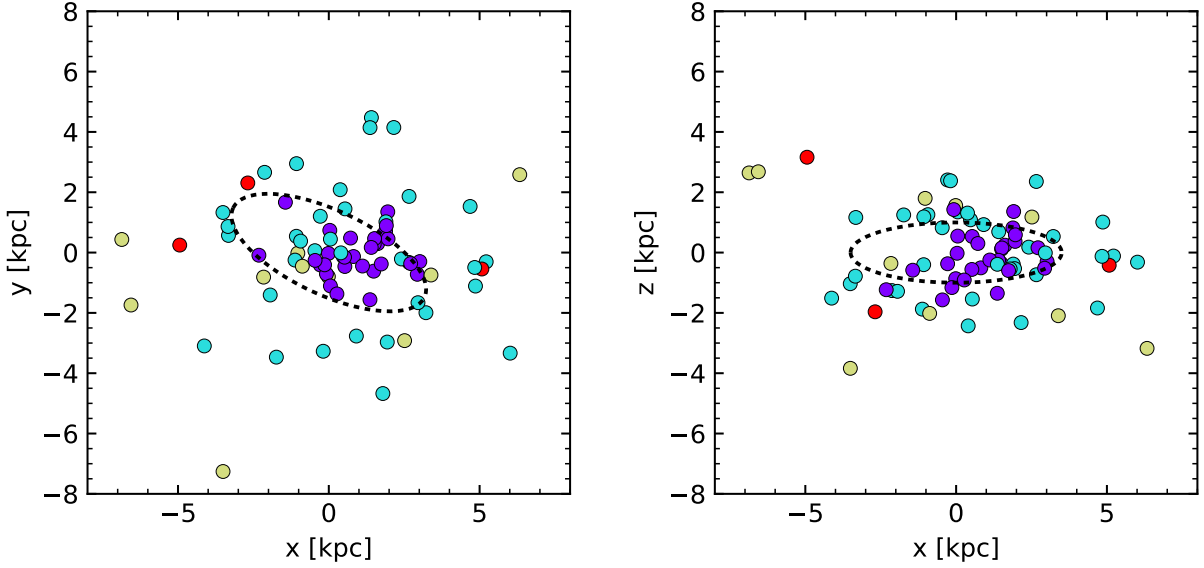


**Figure 7.** Spatial distribution of the GCs in the  $x - y$  (left panel) and  $x - z$  (right panel) projection. The colours are the same as in Figure 6 and indicate the stellar component to which GCs are associated. The black dashed line shows the size of the Galactic bar.

**Table 6.** Classification of GCs based on dynamical properties, assuming their maximum membership probability.

Component	Clusters		
Bulge/Bar	BH 261	NGC 6401	NGC 6637
	Djorg 2	NGC 6440	NGC 6642
	ESO452SC11	NGC 6522	NGC 6717
	HP 1	NGC 6528	Terzan 1
	Liller 1	NGC 6540	Terzan 2
	NGC 6256	NGC 6553	Terzan 4
	NGC 6266	NGC 6558	Terzan 5
	NGC 6304	NGC 6569	Terzan 6
	NGC 6342	NGC 6624	Terzan 9
	NGC 6380	NGC 6626	
Thick disk	Djorg 1	NGC 6388	NGC 6712
	Lynga 7	NGC 6362	NGC 6723
	Mercer 5	NGC 6366	NGC 6752
	NGC 5927	NGC 6402	NGC 6760
	NGC 6139	NGC 6441	NGC 6838
	NGC 6144	NGC 6453	Palomar 6
	NGC 6171	NGC 6517	Palomar 7
	NGC 6273	NGC 6535*	Palomar 8
	NGC 6293	NGC 6539	Terzan 12
	NGC 6316	NGC 6541	Terzan 3
	NGC 6325	NGC 6544	Ton 2
	NGC 6352	NGC 6638	
	NGC 6355	NGC 6652	
Inner Halo	NGC 104	NGC 6356	Palomar 11
Outer Halo	NGC 6284*	NGC 6681	Terzan 10
	NGC 6287	NGC 6809	NGC 6333*

\*GCs that its classification changes with  $\Omega_b$ .

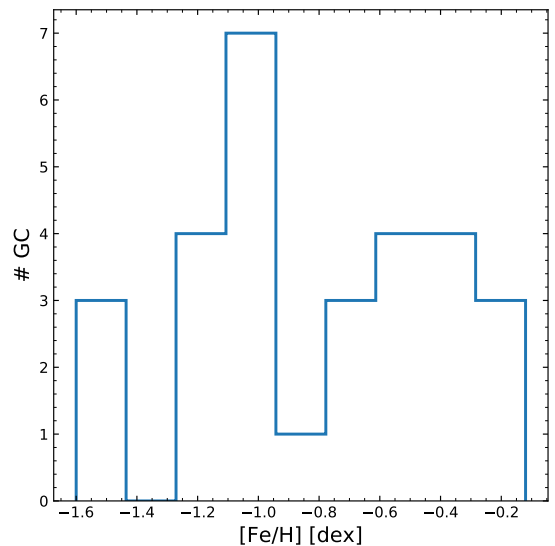


**Figure 8.** Metallicity distribution of bulge globular clusters.

## 7 CONCLUSIONS

Combining accurate absolute PMs from Gaia DR2 with distances from RR Lyrae and/or CMD when available, and radial velocities from spectroscopy, we were able to construct the orbits of 78 GCs among the most centrally located in the

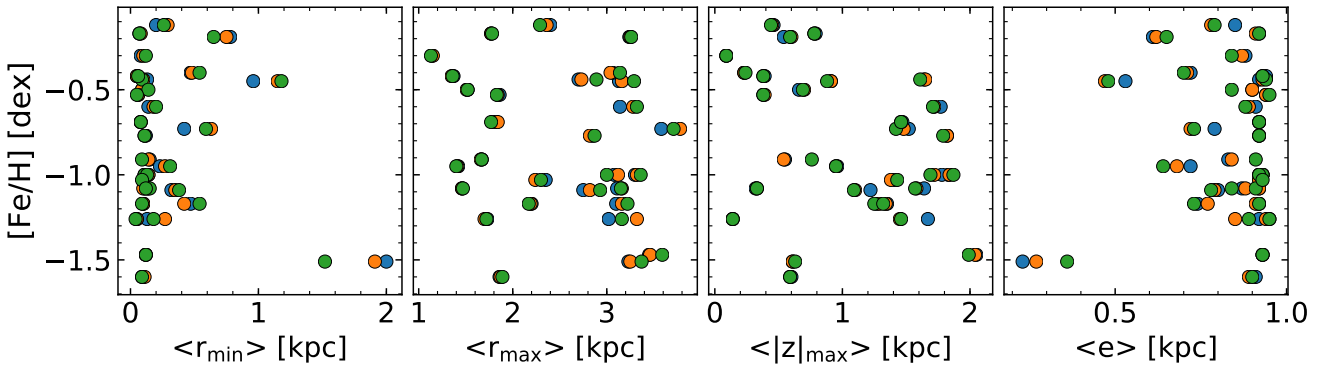


**Figure 9.** Metallicity of bulge globular clusters as function of the median value of perigalactic distance  $\langle r_{min} \rangle$  (first panel), apogalactic distance  $\langle r_{max} \rangle$  (second panel), maximum distance from the Galactic plane  $\langle |z|_{max} \rangle$  (third panel), and eccentricity  $\langle e \rangle$  (fourth panel), for  $\Omega_b = 40$  (blue), 45 (orange) , and 50 (green)  $\text{km s}^{-1} \text{kpc}^{-1}$ .

**Table 7.** Bulge GC orbits that follow the Galactic bar for different pattern speed.

Cluster	Orbits following the bar (%)		
	$\Omega_b = 40$	$\Omega_b = 45$	$\Omega_b = 50$
BH 261	6.2	6.9	8.9
Djorg 2	0.0	0.1	0.0
ESO452SC11	0.0	0.2	0.0
HP 1	0.2	0.4	0.8
Liller 1	38.2	32.1	28.1
NGC 6256	9.0	19.7	36.1
NGC 6266	13.1	9.9	8.3
NGC 6304	27.8	38.1	38.4
NGC 6342	1.0	3.1	3.5
NGC 6380	0.7	0.9	0.3
NGC 6401	0.7	0.7	1.4
NGC 6440	11.3	9.1	7.5
NGC 6522	97.0	95.3	94.7
NGC 6528	44.0	24.0	7.8
NGC 6540	23.1	18.2	12.9
NGC 6553	65.2	63.3	57.0
NGC 6558	19.3	12.5	6.9
NGC 6569	2.0	2.6	3.1
NGC 6624	0.3	0.0	0.1
NGC 6626	0.4	0.1	0.5
NGC 6637	1.3	4.2	4.4
NGC 6642	7.2	2.8	2.1
NGC 6717	0.7	0.8	0.7
Terzan 1	2.0	2.3	1.6
Terzan 2	0.0	0.0	0.0
Terzan 4	19.6	15.1	13.7
Terzan 5	32.8	25.0	12.3
Terzan 6	1.7	2.1	0.5
Terzan 9	87.7	81.8	73.1

Galaxy, using a Galactic bar potential. Most sample clusters are located in the innermost region of the MW.

We generate a set of initial conditions for each cluster using Monte Carlo simulations, taking into account the uncertainties from the heliocentric distance and kinematic data of the clusters. We calculated the average value of the orbital parameters such as the perigalactic and apogalactic

distances, the maximum vertical excursion from the Galactic plane, and the eccentricity. Through the dynamical properties of the orbits, apogalactic distance and the maximum height from the plane, we applied a clustering technique to estimate the membership probability that each cluster has to be part of different stellar populations: bulge/bar, thick disk, inner halo, or outer halo.

Given that in the inner part of the MW, most of Galactic components overlap, one of the goals of this study was to identify which among the bulge GCs classified as such by [Bica et al. \(2016\)](#), are confined in the bulge/bar region. In a few cases, like Djorg 1 and Terzan 10, they are identified as halo intruders in the Galactic bulge ([Ortolani et al. 2019a](#)), and with our analysis, we confirm that they are in fact contaminating the bulge GC population. Others in the same case are NGC 6316, NGC 6355, Ton 2, Palomar 6, and NGC 6723, provided that their distances are confirmed. In terms of dynamical properties, the orbital characteristics of the GCs identified to be part of the bulge/bar are distinct from those in the thick disk/inner halo according to the present classification criteria.

The GCs are very old, whereas the bar likely formed later. In the already seminal paper by [Sheth et al. \(2008\)](#), it was shown that whereas 65% of the present-day luminous spiral galaxies have bars, at redshift  $z \sim 0.84$  (about 6 Gyr ago), this fraction drops to 20%. From a fully cosmological simulation, [Buck et al. \(2018\)](#) suggest that the Galaxy's bar formed  $8 \pm 2$  Gyr ago. Similarly, [Bovy et al. \(2019\)](#) used chemical abundances from the *Apache Point Observatory Galactic Evolution Experiment* (APOGEE) survey, and kinematical information from the Gaia collaboration, and concluded that the Galactic bar formed  $\sim 8$  Gyr ago. Therefore, the fact that the GCs are in the bar, probably indicates that they were confined in the bar when the latter formed.

Most of the bulge GCs are confined in the bar region but are not supporting the bar structure, the seven clusters that are supporting the bar do not necessarily support the X-shape. In particular Terzan 5, that is confined in the bar, was revealed to have multiple populations in a range of metallicities and ages ([Origlia et al. 2019](#), and references therein), suggesting this object to be the nucleus of a dwarf galaxy.

Currently, we have very accurate proper motions from Gaia, and radial velocities from high resolution spectroscopy, however in most cases there are no accurate distance determinations, and they are crucial to characterize the orbits. Further efforts on distance derivation from accurate CMDs and/or RR Lyrae, are greatly needed.

## ACKNOWLEDGEMENTS

We acknowledge the anonymous referee for the detailed review and for the helpful suggestions, which allowed us to improve the manuscript. APV acknowledges the FAPESP postdoctoral fellowship no. 2017/15893-1. BB and EB acknowledge grants from the Brazilian agencies CAPES - Finance code 001, CNPq and FAPESP. SO acknowledges partial support by the Università degli Studi di Padova Progetto di Ateneo CPDA141214 and BIRD178590 and by INAF under the program PRIN-INAF2014. SOS acknowledges the FAPESP PhD fellowship no. 2018/22044-3. APV and SOS acknowledge the DGAPA-PAPIIT grant IG100319. “This work has made use of data from the European Space Agency (ESA) mission Gaia (<https://www.cosmos.esa.int/gaia>), processed by the Gaia Data Processing and Analysis Consortium (DPAC, <https://www.cosmos.esa.int/web/gaia/dpac/consortium>). Funding for the DPAC has been provided by national institutions, in particular the institutions participating in the Gaia Multilateral Agreement.”

## REFERENCES

- Aguilar, L., Hut, P., Ostriker, J.P. 1988, ApJ, 335, 720  
 Armandroff, T.E., 1989, AJ, 97, 375  
 Barbuy, B., Bica, E., & Ortolani, S. 1998, A&A, 333, 117  
 Barbuy, B., Cantelli, E., Vemado, A., et al. 2016, A&A, 591, A53  
 Barbuy, B., Chiappini, C., Cantelli, E., et al. 2014, A&A, 570, A76  
 Barbuy, B., Chiappini, C., & Gerhard, O. 2018a, ARA&A, 56, 223  
 Barbuy, B., Muniz, L., Ortolani, S., et al. 2018b, A&A, 619, A178  
 Baumgardt, H., Hilker, M., Sollima, A., & Bellini, A. 2019, MNRAS, 482, 5138  
 Bica, E., Bonatto, C., Barbuy, B., & Ortolani, S. 2006, A&A, 450, 105  
 Bica E., Ortolani S., Barbuy B., 2016, PASA, 33, e028  
 Bica, E., Pavani, D. B., Bonatto, C. J., & Lima, E. F. 2019, AJ, 157, 12  
 Bissantz, N., Englmaier, P., & Gerhard, O. 2003, MNRAS, 340, 949  
 Bland-Hawthorn, J., Gerhard, O. 2016, ARA&A, 54, 529  
 Buck, T., Ness, M.K., Obreja, A., Maccio, A.V., Dutton, A.A. 2018, ApJ, 861, 88  
 Bovy, J., Leung, H. W., Hunt, J. A. S., et al. 2019, arXiv:1905.11404  
 Caldwell, N., & Romanowsky, A. J. 2016, ApJ, 824, 42  
 Côté, P. 1999, AJ, 118, 406  
 Dias, B., Barbuy, B., Saviane, I., et al. 2016, A&A, 590, A9  
 Dinescu, D. I., Girard, T. M., van Altena, W. F., & López, C. E. 2003, AJ, 125, 1373  
 Frenk, C., White, S. 1982, MNRAS, 198, 173  
 Freudenreich, H. T. 1998, ApJ, 492, 495  
 Gaia Collaboration, A. G. A. Brown, A. Vallenari, T. Prusti, J. H. J. de Bruijne, C. Babusiaux, C. A. L. Bailer-Jones and et al. (2018a) Gaia Data Release 2, A&A 616, pp. A1.  
 Gaia Collaboration, Helmi, A., van Leeuwen, F., et al. 2018b, A&A, 616, A12  
 Gardner, E., & Flynn, C. 2010, MNRAS, 405, 545  
 Harris, W. E. 1996, AJ, 112, 1487  
 Hilker, M., Baumgardt, H., Sollima, A., et al. 2019, arXiv e-prints, arXiv:1908.02778  
 Irrgang, A., Wilcox, B., Tucker, E., & Schiefelbein, L. 2013, A&A, 549, A137  
 Kent, S. M., Dame, T. M., & Fazio, G. 1991, ApJ, 378, 131  
 Kerber, L. O., Libralato, M., Souza, S. O., et al. 2019, MNRAS, 484, 5530  
 Kerber, L. O., Nardiello, D., Ortolani, S., et al. 2018, ApJ, 853, 15  
 Minniti, D. 1995, AJ, 109, 1663  
 Minniti, D., Alonso-García, J., & Pullen, J. 2017b, Research Notes of the American Astronomical Society, 1, 54  
 Minniti, D., Geisler, D., Alonso-García, J., et al. 2017a, ApJ, 849, L24  
 Miyamoto, M., & Nagai, R. 1975, PASJ, 27, 533  
 Navarro, J. F., Frenk, C. S., & White, S. D. M. 1997, ApJ, 490, 493  
 Origlia, L., Mucciarelli, A., Fiorentino, G. et al. 2019, ApJ, 871, 114  
 Ortolani, S., Bica, E., & Barbuy, B. 1995, A&A, 296, 680  
 Ortolani, S., Nardiello, D., Pérez-Villegas, A., Bica, E., & Barbuy, B. 2019a, A&A, 622, A94  
 Ortolani, S., Held, E. V., Nardiello, D., et al. 2019b, A&A, 627, A145  
 Pasquato, M., Chung, C. 2019, astro-ph:1901.05354  
 Pedregosa, F., Varoquaux, G., Gramfort, A., et al., 2011, JMLR, 12, 2825–2830  
 Pérez-Villegas, A., Portail, M., Wegg, C., & Gerhard, O. 2017, ApJ, 840, L2  
 Pérez-Villegas, A., Rossi, L., Ortolani, S., et al. 2018, Publ. Astron. Soc. Australia, 35, e021  
 Pfenniger, D. 1984, A&A, 134, 373  
 Portail, M., Wegg, C., Gerhard, O., & Martínez-Valpuesta, I. 2015a, MNRAS, 448, 713  
 Portail, M., Wegg, C., & Gerhard, O. 2015b, MNRAS, 450, L66  
 Portail, M., Gerhard, O., Wegg, C., & Ness, M. 2017, MNRAS, 465, 1621  
 Rattenbury, N. J., Mao, S., Sumi, T., & Smith, M. C. 2007, MNRAS, 378, 1064  
 Rossi, L. J. 2015a, Astronomy and Computing, 12, 11  
 Rossi, L. J., Ortolani, S., Barbuy, B., Bica, E., & Bonfanti, A. 2015b, MNRAS, 450, 3270  
 Saito, R. K., Hempel, M., Minniti, D., et al. 2012, A&A, 537, A107  
 Sheth K., et al., 2008, ApJ, 675, 1141  
 Schönrich, R., Binney, J., & Dehnen, W. 2010, MNRAS, 403, 1829  
 Smith, R., Flynn, C., Candlish, G. N., Fellhauer, M., & Gibson, B. K. 2015, MNRAS, 448, 2934  
 Valenti, E., Ferraro, F. R., & Origlia, L. 2007, AJ, 133, 1287  
 Valenti, E., Ferraro, F. R., & Origlia, L. 2010, MNRAS, 402, 1729  
 Vasiliev, E. 2019, MNRAS, 484, 2832  
 Vásquez, S., Saviane, I., Held, E. V., et al. 2018, A&A, 619, A13  
 Wegg, C., & Gerhard, O. 2013, MNRAS, 435, 1874  
 Weiner, B. J., & Sellwood, J. A. 1999, ApJ, 524, 112  
 Zinn, R. 1980, ApJ, 241, 602  
 Zinn, R. 1985, ApJ, 293, 424

This paper has been typeset from a Te<sub>X</sub>/La<sub>T</sub>E<sub>X</sub> file prepared by the author.